Chemical Science

ROYAL SOCIETY OF CHEMISTRY

EDGE ARTICLE

View Article Online
View Journal | View Issue

Cite this: *Chem. Sci.*, 2021, **12**, 7848

All publication charges for this article have been paid for by the Royal Society of Chemistry

Received 3rd February 2021
Accepted 24th April 2021

DOI: 10.1039/d1sc00691f

rsc.li/chemical-science

Biocompatible metal–organic frameworks for the storage and therapeutic delivery of hydrogen sulfide†

Faith E. Chen, ‡[a] Ruth M. Mandel, ‡[a] Joshua J. Woods, [ab] Jung-Hoon Lee, [c] Jaehwan Kim, [a] Jesse H. Hsu,[a] José J. Fuentes-Rivera, [a] Justin J. Wilson [a] and Phillip J. Milner *[a]

Hydrogen sulfide (H_2S) is an endogenous gasotransmitter with potential therapeutic value for treating a range of disorders, such as ischemia-reperfusion injury resulting from a myocardial infarction or stroke. However, the medicinal delivery of H_2S is hindered by its corrosive and toxic nature. In addition, small molecule H_2S donors often generate other reactive and sulfur-containing species upon H_2S release, leading to unwanted side effects. Here, we demonstrate that H_2S release from biocompatible porous solids, namely metal–organic frameworks (MOFs), is a promising alternative strategy for H_2S delivery under physiologically relevant conditions. In particular, through gas adsorption measurements and density functional theory calculations we establish that H_2S binds strongly and reversibly within the tetrahedral pockets of the fumaric acid-derived framework MOF-801 and the mesaconic acid-derived framework Zr-mes, as well as the new itaconic acid-derived framework CORN-MOF-2. These features make all three frameworks among the best materials identified to date for the capture, storage, and delivery of H_2S. In addition, these frameworks are non-toxic to HeLa cells and capable of releasing H_2S under aqueous conditions, as confirmed by fluorescence assays. Last, a cellular ischemia-reperfusion injury model using H9c2 rat cardiomyoblast cells corroborates that H_2S-loaded MOF-801 is capable of mitigating hypoxia-reoxygenation injury, likely due to the release of H_2S. Overall, our findings suggest that H_2S-loaded MOFs represent a new family of easily-handled solid sources of H_2S that merit further investigation as therapeutic agents. In addition, our findings add Zr-mes and CORN-MOF-2 to the growing lexicon of biocompatible MOFs suitable for drug delivery.

Introduction

Hydrogen sulfide (H_2S) is a colorless, flammable gas with a distinctive "rotten-egg" odor that is pervasive in industrial processes such as petroleum refining, natural gas processing, and wastewater treatment.[1,2] Because H_2S is an irritant to respiratory linings and a chemical asphyxiant, it has a recommended Immediately Dangerous to Life and Health (IDLH) value of 100 ppm, above which prolonged exposure can be fatal. In addition to being toxic to humans at high concentrations, H_2S impurities in gas streams are highly corrosive to piping and other equipment.[3,4] In spite of its toxic and corrosive nature, H_2S is also an important gasotransmitter in mammals with proposed roles in calcium homeostasis, long-term potentiation, and mediation of oxidative stress.[5–7] As such, H_2S has been invoked as a potential therapeutic for numerous disorders, including bone disease, brain injury, inflammation, Parkinson's disease, high blood pressure, cancer, and ischemia-reperfusion injury.[8–15]

The toxicity and flammability of H_2S limit the viability of inhalation as a therapeutic delivery pathway.[9] Indeed, studies regarding the potential biological role and therapeutic value of H_2S rarely employ this gas directly. Instead, researchers have designed small molecule donors that decompose to generate H_2S or related species under physiological conditions.[9,10,12,13,16,17] However, the application of these donors is complicated by the concomitant production of reactive byproducts and other sulfur-based species upon H_2S release.[9] A promising alternative strategy is to design biocompatible porous solids capable of storing and controllably releasing gaseous H_2S, avoiding the formation of biologically-active byproducts. In particular, metal–organic frameworks (MOFs),

[a]*Department of Chemistry and Chemical Biology, Cornell University, Ithaca, NY 14850, USA. E-mail: pjm347@cornell.edu*

[b]*Robert F. Smith School for Chemical and Biomolecular Engineering, Cornell University, Ithaca, NY 14850, USA*

[c]*Computational Science Research Center, Korea Institute of Science and Technology (KIST), Seoul 02792, Republic of Korea*

† Electronic supplementary information (ESI) available: Synthetic, computational, and biological assay details. See DOI: 10.1039/d1sc00691f

‡ Contributed equally.

which are porous materials constructed from organic "linkers" and inorganic "nodes," are promising materials for the controlled delivery of bioactive molecules,[18–20] such as the gasotransmitter nitric oxide (NO).[21] The chemical tunability of MOFs achievable through linker modification and surface functionalization is a promising feature which could potentially enable control over the rate and location of H_2S delivery.[22] Nonetheless, the potential application of MOFs as H_2S donors in medicine remains almost completely unexplored.[22,23]

To be useful for H_2S delivery *in vivo*, MOF-based platforms must meet several criteria, including: (1) construction from non-toxic metals and linkers; (2) stability towards H_2S; (3) high H_2S capacities with controlled release under physiological conditions; and (4) stability under physiological conditions (*e.g.*, serum at 37 °C). However, *none of the MOFs that have been studied for H_2S adsorption to date fulfill all of these criteria*, as many are limited by framework destruction upon irreversible H_2S binding,[22–30] low capacities,[26,31] poor biocompatibility, or harsh H_2S desorption conditions.[2,23,24,30,32] In addition, many previously studied MOFs are constructed from toxic metals (*e.g.*, Ni, Cr)[22,30] or complex organic linkers[33] that could lead to unwanted side effects *in vivo*. For example, the only MOF that has been explored for therapeutic H_2S delivery to date, namely, Zn-MOF-74, fails to meet several of these criteria.[23] We have found that H_2S adsorption in Zn-MOF-74 is completely irreversible, which precludes its application for H_2S delivery. This framework was also found to be highly toxic to HeLa cells (see ESI or ESI Section 15† for details). Therefore, there remains a critical need to identify biocompatible MOFs that display strong yet reversible H_2S adsorption for application as next-generation H_2S donors.

A promising strategy to identify new MOFs capable of reversibly adsorbing H_2S is to leverage its properties as a hydrogen-bond donor and weak hydrogen-bond acceptor, similar to water.[34] As such, we were inspired by the recent deluge of MOFs designed for reversible water capture[35–38] to identify potential frameworks for H_2S storage. In particular, we hypothesized that the surprisingly strong binding of water ($-\Delta H_{ads} \approx 60$ kJ mol^{-1}) in $Zr_6O_4(OH)_4$(fumarate)$_6$ or MOF-801 (Fig. 1, left), which is due to ordered hydrogen-bonding interactions within the tetrahedral cavities,[39] may translate to strong binding of H_2S within this MOF as well. In addition, Zr is a non-toxic metal[40] and fumaric acid occurs naturally as part of the Krebs cycle,[41,42] suggesting that MOF-801 and closely related frameworks should also be biocompatible.[43] Here, through combined experimental and computational analyses we demonstrate that MOF-801, as well as the related biocompatible mesaconate-based framework Zr-mes[44,45] and itaconate-based framework CORN-MOF-2 (CORN = Cornell University)[46,47] undergo strong but reversible adsorption of H_2S with minimal framework degradation (Fig. 1). In addition, these frameworks are capable of delivering H_2S under physiologically relevant conditions, allowing for the therapeutic benefits of H_2S to be accessed using easily-handled solids. Taken together, these features make the frameworks described here promising H_2S donors for biomedical applications.

Results and discussion

Preparation of MOFs

The MOFs $Zr_6O_4(OH)_4$(fumarate)$_6$ and $Zr_6O_4(OH)_4$(mesaconate)$_6$ are also known as MOF-801 (ref. 39) and Zr-mes,[44] respectively. Herein, we refer to these frameworks as Zr-fum and Zr-mes, respectively, for clarity. Following procedures adapted from the literature, we prepared Zr-fum and Zr-mes under solvothermal conditions on 10 mmol scale (see ESI Sections 3–6† for details). Specifically, these frameworks were synthesized from $ZrOCl_2 \cdot 8H_2O$ and the corresponding dicarboxylic acid in either *N*,*N*-dimethylformamide (Zr-fum-DMF,[39] Zr-mes-DMF[44]) or water (Zr-fum-H_2O,[48] Zr-mes-H_2O[48]) using formic acid as a modulator. After optimization, 30 equivalents of formic acid were found to produce Zr-fum and Zr-mes with high crystallinity, as determined by powder X-ray diffraction (PXRD; ESI Fig. S1 and S2†). Notably, higher concentrations of formic acid led to the formation of significant impurities.

The PXRD patterns of solvated Zr-fum and Zr-mes prepared in DMF and in H_2O are shown in Fig. 2. The PXRD patterns for Zr-fum-DMF and Zr-fum-H_2O match the predicted pattern corresponding to the single-crystal X-ray diffraction (SCXRD) structure of MOF-801.[39] Likewise, the patterns for Zr-mes match the predicted pattern based on the density functional theory (DFT)-calculated ideal structure of this framework (see ESI Section 14† for details). The Langmuir surface areas determined from 77 K N_2 adsorption isotherms of all four frameworks are in good agreement with previously reported values (ESI Fig. S7, S13, S19, and S25†). Unlike Zr-fum-H_2O, Zr-mes-H_2O was found to undergo partial amorphization upon complete desolvation under high vacuum (<10 μbar) at 100 °C, although this did not impact its porosity. Notably, synthesis under aqueous conditions produced nanocrystals of Zr-fum-H_2O less than 100 nm in size (ESI Fig. S15†), suitable for applications in medicine,[49] whereas synthesis in DMF produced larger crystallites approximately 500 nm in size (ESI Fig. S9†). The framework Zr-mes was obtained as crystallites of intermediate size (100–200 nm) under both sets of conditions (ESI Fig. S21 and S27†). Owing to the similar properties of frameworks prepared in water and in DMF, we employed Zr-fum-H_2O and Zr-mes-H_2O for subsequent studies to bypass the use of toxic DMF.

After preparing Zr-fum-H_2O and Zr-mes-H_2O, we next investigated whether the naturally-derived and inexpensive dicarboxylic acid itaconic acid[46,47] can be used to synthesize an isostructural MOF, which we term CORN-MOF-2 and refer to as Zr-ita herein for consistency (Fig. 1; see ESI Sections 7 and 8† for details). Produced *via* the fermentation of carbohydrates by fungi from the genus *Aspergillus*, itaconic acid is a desirable linker because of its very low cost and lack of toxicity.[46] Unfortunately, solvothermal synthesis using $ZrCl_4$ and itaconic acid in DMF produced amorphous material, as confirmed by PXRD (Fig. 2). Several acid modulators were evaluated to enhance the crystallinity of Zr-ita-DMF, including acetic acid, L-proline, concentrated HCl, pivalic acid, and formic acid, but none led to crystalline MOF. In addition, N_2 sorption isotherms of Zr-ita-DMF prepared without an acid modulator revealed minimal

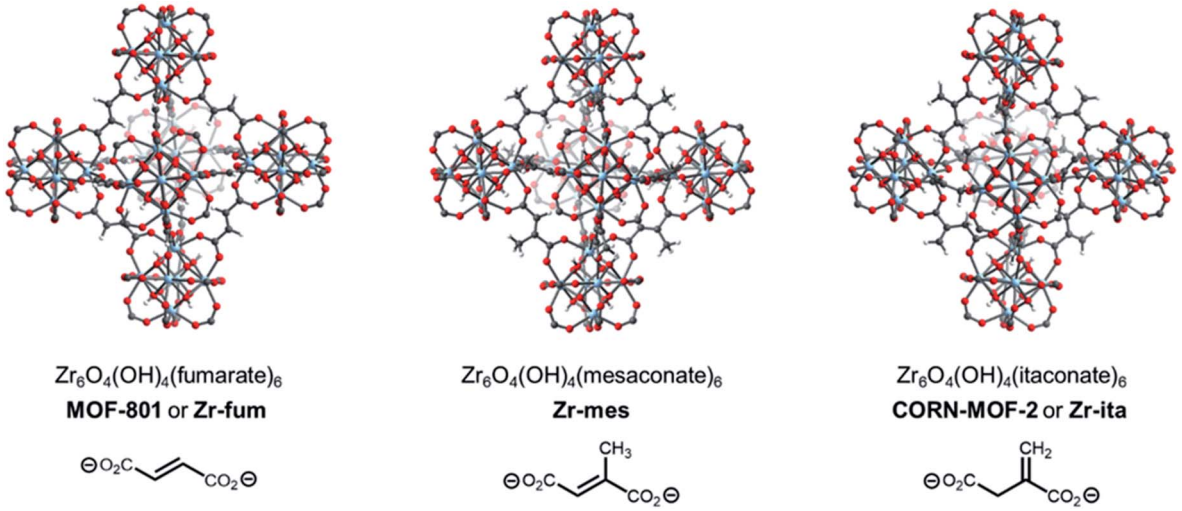

Fig. 1 Density functional theory-calculated ideal structures of known and new sustainably-derived metal–organic frameworks prepared from fumaric, mesaconic, and itaconic acid as part of this work. Gray, white, red, and pale blue spheres correspond to carbon, hydrogen, oxygen, and zirconium, respectively.

porosity and a Brunauer–Emmett–Teller (BET) surface area of only 33 $m^2\ g^{-1}$ (ESI Fig. S30†). Insight into the poor quality of amorphous Zr-ita-DMF was obtained from ^{1}H-NMR spectra of samples digested using a saturated K_3PO_4/D_2O solution in DMSO-d_6 (ESI Fig. S31†). Peaks due to itaconate and residual solvent were observed as expected. However, additional peaks ascribed to the isomeric mesaconate were also observed. We hypothesize that basic *N*,*N*-dimethylamine generated by the hydrolysis of DMF mediates the isomerization of itaconate to mesaconate during framework self-assembly, leading to an amorphous structure. In addition, residual DMF was observed by ^{1}H-NMR even after extensive soaking in tetrahydrofuran. Therefore, the significant linker isomerization and difficulty in removing DMF from the pores together account for the low surface area of Zr-ita-DMF.

We hypothesized that the key to preparing high-quality Zr-ita was to avoid the use of base during MOF synthesis. Consistently, employing water as the solvent instead of DMF produced semi-crystalline Zr-ita-H_2O for the first time (Fig. 2). The modest crystallinity of Zr-ita-H_2O compared to Zr-fum-H_2O and Zr-mes-H_2O is likely due to the sp^3-hybridized carbon in the backbone of this flexible linker. Because of these characteristics, Zr-ita-H_2O is likely an amorphous MOF (aMOF), which have found application for toxic gas capture and drug delivery.[50] Because the DFT-calculated structure of Zr-ita-H_2O is idealized and does not account for linker flexibility, the PXRD pattern simulated from this structure in Fig. 1 does not reflect the amorphous nature of Zr-ita-H_2O. When prepared on 10 mmol scale, Zr-ita-H_2O exhibited improved porosity compared to Zr-ita-DMF, with a 77 K N_2 BET surface area of 235 ± 2 $m^2\ g^{-1}$ and a Langmuir surface area of 487 ± 22 $m^2\ g^{-1}$ (ESI Fig. S35†). Marked hysteresis was also observed upon N_2 desorption in Zr-ita-H_2O. Analysis of the pore size distribution from the N_2 sorption isotherm revealed micropores approximately 6.6 Å in

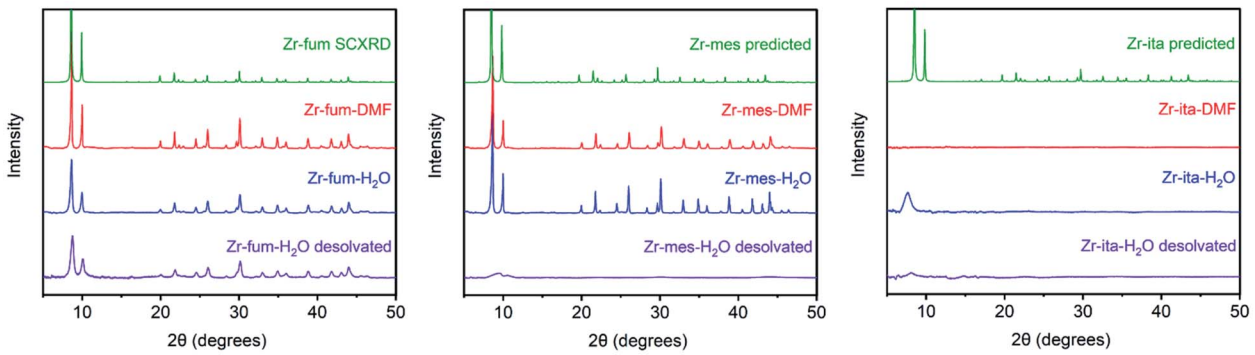

Fig. 2 Comparison of PXRD patterns of Zr-fum, Zr-mes, and Zr-ita prepared in DMF and in water. The patterns for MOFs prepared in DMF (red) and H_2O (blue) were obtained after activation at 100 °C under vacuum (<100 mbar) using a Schlenk line and were found to still contain ethanol by ^{1}H-NMR digestion. Further desolvation at 100 °C under stronger vacuum (<10 μbar) led to partial amorphization of Zr-mes and Zr-ita, but not Zr-fum (purple). The predicted patterns based on the previously reported single crystal X-ray diffraction pattern of Zr-fum and from the DFT-calculated ideal structures of Zr-mes and Zr-ita are included for reference (green).

diameter (ESI Fig. S39†), as expected based on the idealized structure, along with mesopores 20–100 Å in size. Thus, we attribute the observed hysteresis to mesoporous defects or cavities between particles. Consistent with the hypothesis outlined above, the ^{1}H-NMR spectra of Zr-ita-H_2O digested using a saturated K_3PO_4/D_2O solution in DMSO-d_6 revealed only resonances attributed to the itaconate linker, residual formate from defect sites, and solvent (ESI Fig. S36†). To further illustrate the scalability of Zr-ita-H_2O, we prepared this new framework on 0.5 mol scale, resulting in a total yield of approximately 87 g (73% yield) of activated framework (see ESI Section 8† for details). Thus, Zr-ita-H_2O was employed for subsequent H_2S adsorption studies to compare with Zr-fum-H_2O and Zr-mes-H_2O.

H_2S adsorption in MOFs

After preparing Zr-fum-H_2O, Zr-mes-H_2O, and Zr-ita-H_2O, we next evaluated the reversible H_2S capture performance of all three frameworks by carrying out isothermal adsorption measurements at 25 °C, 40 °C, and 55 °C (Fig. 3; see ESI Section 10† for details). At 25 °C and 1 bar of H_2S, Zr-fum-H_2O displayed the highest H_2S uptake (4.0 mmol g^{-1}, 11 wt%) followed by Zr-mes-H_2O (3.3 mmol g^{-1}, 10 wt%) and Zr-ita-H_2O (1.3 mmol g^{-1}, 4.0 wt%), which trends with the frameworks' respective surface areas. These measurements indicate that Zr-fum-H_2O and Zr-mes-H_2O possess capacities comparable to those in MOFs that undergo (partially) reversible H_2S adsorption under similar conditions, such as UiO-66 (~3.0 mmol g^{-1}; UiO = Universitetet i Oslo),[21] MIL-53 (Al) (~3.5 mmol g^{-1}),[13] MIL-53 (Cr) (~3.5 mmol g^{-1}),[13] and Ga-soc-MOF-1a (~4.5 mmol g^{-1}; soc = square octahedral).[22] Moreover, the relatively smooth overlay of the adsorption and desorption data suggests that H_2S binds reversibly at every temperature (see below for further discussion). Although H_2S adsorption is readily reversible at 25 °C in all three frameworks, they were regenerated at 100 °C under high vacuum (<10 μbar) between experiments for consistency.

To investigate the thermodynamics of H_2S binding in Zr-fum-H_2O, Zr-mes-H_2O, and Zr-ita-H_2O, we fit the adsorption data in Fig. 3 using both dual-site Langmuir and Langmuir–Freundlich models (ESI Fig. S46, S49, S52 and Tables S2–S4†). Although both models provided adequate fits to the data, the empirical Langmuir–Freundlich fits (Fig. 3) were found to be superior and thus were employed for subsequent analysis. The differential enthalpies of adsorption were calculated as a function of isosteric H_2S loading using the Clausius–Clapeyron equation (eqn (1)), in which P_Q is the pressure at a constant uptake Q, ΔH_{ads} is the differential enthalpy of adsorption, R is the ideal gas constant, T is the temperature, and c is a constant.

$$\ln(P_Q) = \left(\frac{\Delta H_{ads}}{R}\right)\left(\frac{1}{T}\right) + c \quad (1)$$

The differential enthalpies of adsorption ($-\Delta H_{ads}$) for all three frameworks are included in Fig. 4. The low-coverage adsorption enthalpies follow the trend Zr-ita-H_2O (53.2 ± 0.8 kJ mol^{-1}) > Zr-mes-H_2O (44.7 ± 0.6 kJ mol^{-1}) > Zr-fum-H_2O (32.2 ± 5.6 kJ mol^{-1}). The same trend was observed when the data were fit using dual-site Langmuir models as well (ESI Fig. S46, S49, and S52†). This difference is likely due to the smaller pores of Zr-ita-H_2O and Zr-mes-H_2O, which enable enhanced hydrogen-bonding interactions between H_2S and the

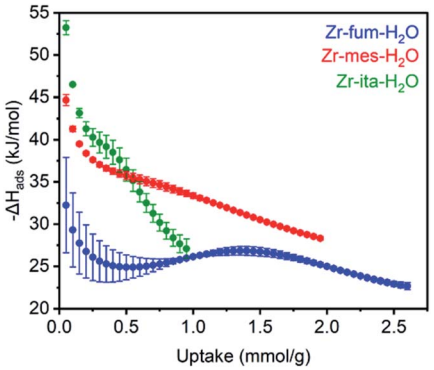

Fig. 4 Differential enthalpies of adsorption ($-\Delta H_{ads}$) for H_2S as a function of uptake for activated Zr-fum-H_2O (blue), Zr-mes-H_2O (red), and Zr-ita-H_2O (green), as determined using the Clausius–Clapeyron equation (eqn (1)) and Langmuir–Freundlich fits in Fig. 3. A data point was considered equilibrated after <0.01% pressure change occurred over a 45 s interval.

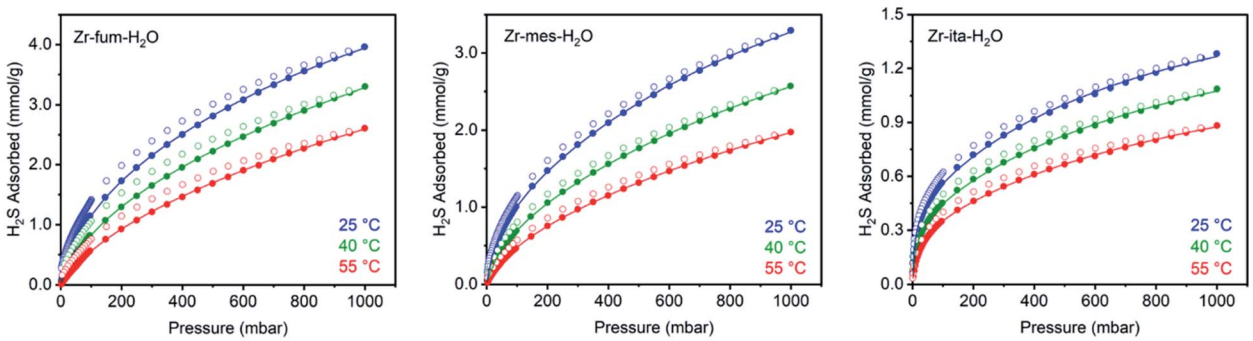

Fig. 3 H_2S adsorption (closed circles) and desorption (open circles) isotherms at 25 °C (blue), 40 °C (green), and 55 °C (red) of activated Zr-fum-H_2O, Zr-mes-H_2O, and Zr-ita-H_2O. Solid lines represent fits of the adsorption data to a Langmuir–Freundlich model. A data point was considered equilibrated after <0.01% pressure change occurred over a 45 s interval.

framework.[31,33,51–53] Consistently, preliminary *in situ* diffuse reflectance infrared Fourier transform spectroscopy (DRIFTS) measurements of H_2S-dosed Zr-fum-H_2O are indicative of hydrogen-bonding interactions between H_2S and the framework upon adsorption (ESI Fig. S106; see ESI Section 16† for details).[52] The data in Fig. 4 are among the first experimentally-derived differential enthalpies of H_2S adsorption in MOFs, and they are comparable to or higher than those predicted computationally for previously-reported frameworks.[24,31,33] The comparatively strong binding of H_2S in Zr-fum-H_2O, Zr-mes-H_2O, and Zr-ita-H_2O bodes well for their ability to store H_2S prior to release upon exchange with water under physiological conditions.

The reversibility of H_2S adsorption and long-term stability towards H_2S are also critical criteria for prospective H_2S-storage materials. As such, we carefully evaluated the stability of Zr-fum-H_2O, Zr-mes-H_2O, and Zr-ita-H_2O towards H_2S in both the gas and solution phases. To characterize the stability of Zr-fum-H_2O, Zr-mes-H_2O, and Zr-ita-H_2O to H_2S in solution, we soaked each MOF in a 0.8 M solution of H_2S in THF at 50 °C for 48 h. Negligible changes in the PXRD patterns, infrared spectra, and ^{1}H-NMR spectra after digestion with a saturated K_3PO_4/D_2O solution were observed for the MOFs after exposure to H_2S in solution, suggesting that, in contrast to Zn-MOF-74, little-to-no framework degradation occurred under these conditions (see ESI Section 11† for details).

Consistent with the desorption data in Fig. 3, the 77 K N_2 Langmuir surface areas of all three MOFs also remained essentially unchanged after exposure to gaseous H_2S at 25 °C (Fig. 5). In contrast, water vapor binds strongly and only semi-reversibly to all three frameworks, leading to a partial reduction in their Langmuir surface areas after exposure to H_2O vapor at 35 °C (see ESI Section 9† for details). To corroborate the reversibility of H_2S adsorption in Zr-fum-H_2O, Zr-mes-H_2O, and Zr-ita-H_2O, we also carried out cycling experiments in which the MOFs were repeatedly exposed to approximately 1 bar of H_2S at 30 °C followed by desorption at 100 °C under vacuum (Fig. 6). The H_2S cycling capacities of all three frameworks remained relatively constant over ten cycles, decreasing by only 3% for Zr-fum-H_2O, 8% for Zr-mes-H_2O, and 6% for Zr-ita-H_2O, respectively. In addition, 77 K N_2 adsorption measurements confirmed that the Langmuir surface areas of all three frameworks

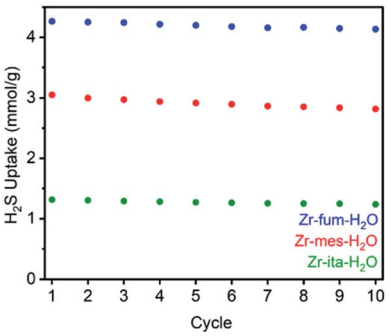

Fig. 6 Cycling capacities for H_2S adsorption (1 bar, 30 °C) in Zr-fum-H_2O, Zr-mes-H_2O, and Zr-ita-H_2O. The samples were regenerated at 100 °C under high vacuum (<10 μbar) between cycles.

remained high after repeated cycling of H_2S, and characterization by PXRD and ^{1}H-NMR after digestion with a saturated K_3PO_4/D_2O solution confirmed that minimal degradation occurred during H_2S cycling (see ESI Section 12† for details). Last, the lack of residual sulfur species in Zr-fum-H_2O that had been exposed to H_2S and subsequently activated under vacuum was confirmed by X-ray photoelectron spectroscopy (ESI Fig. S102 and S103†). Together, these experimental measurements confirm that H_2S adsorbs reversibly and non-destructively within Zr-fum-H_2O, Zr-mes-H_2O, and Zr-ita-H_2O, in contrast to Zn-MOF-74.[22] Indeed, the excellent performance of these materials upon H_2S cycling places them among the upper echelon of frameworks that have been studied for H_2S capture and/or delivery to date. Importantly, the lack of degradation upon H_2S adsorption in these materials indicates that they should be capable of cleanly delivering pure H_2S that is uncontaminated by any other sulfur-containing species.[9]

Due to the microcrystalline nature of the MOFs studied herein, we were unable to study the binding modes of H_2S within each MOF by single-crystal X-ray diffraction. Thus, we turned to density functional theory (DFT) calculations to probe the structure of H_2S bound within Zr-fum, Zr-mes, and Zr-ita (Fig. 7; see ESI Section 14† for details). Calculations were carried out using a plane-wave basis and projector augmented-wave (PAW) pseudopotentials and corrected for dispersive interactions.[54–56] The fidelity of our calculations was confirmed

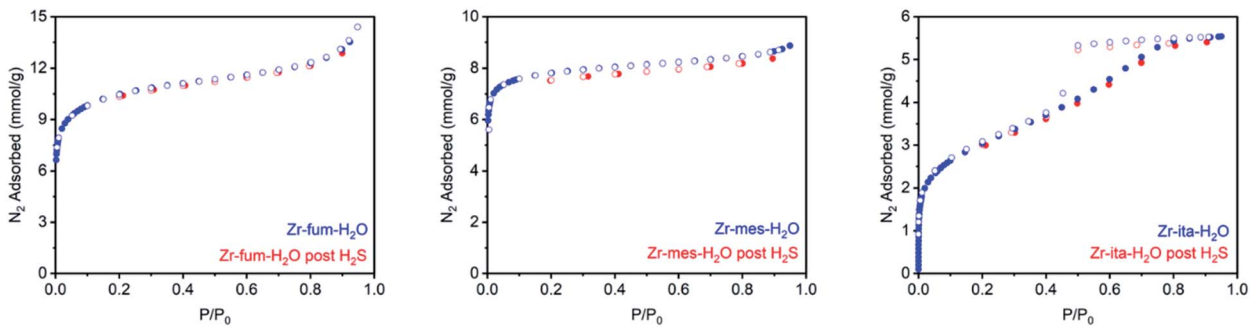

Fig. 5 77 K N_2 adsorption isotherms of activated Zr-fum-H_2O, Zr-mes-H_2O, and Zr-ita-H_2O before (blue) and after treatment with H_2S at 25 °C (red). After H_2S adsorption, the MOFs were regenerated at 100 °C under vacuum (<10 μbar) for 48 h.

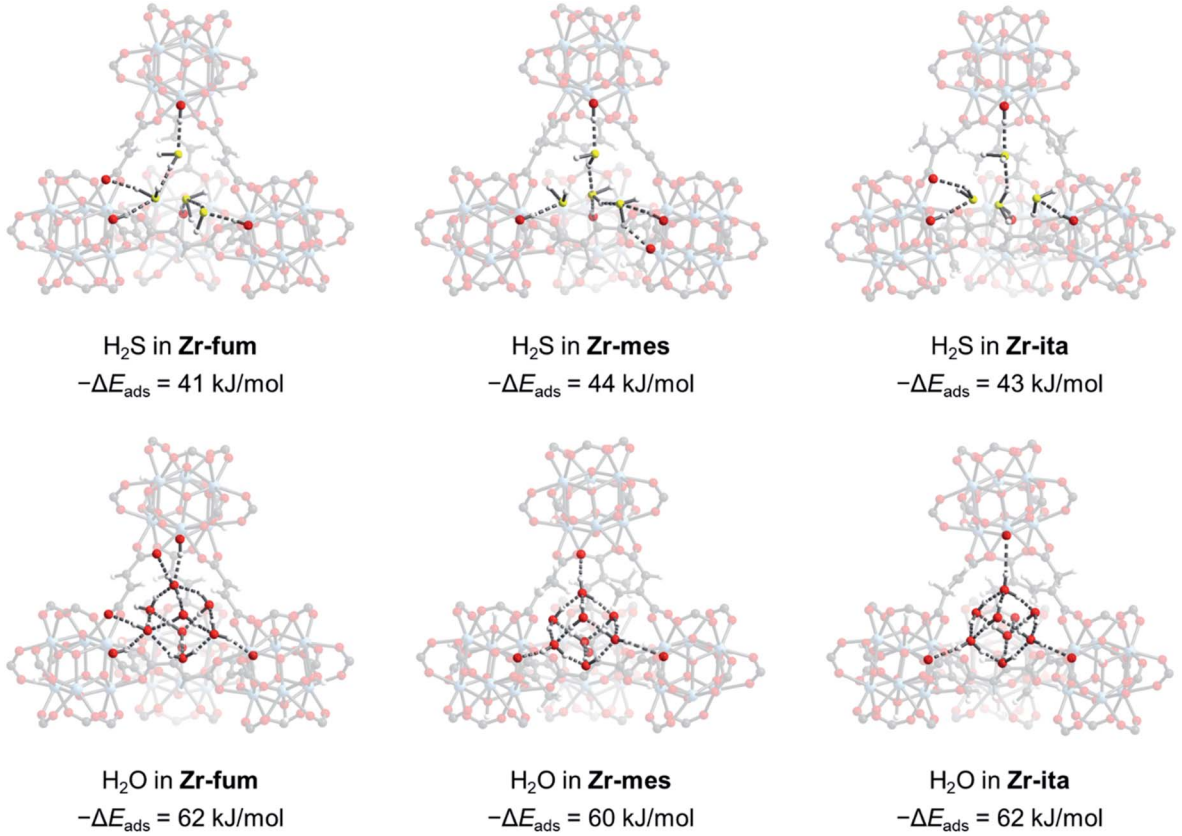

Fig. 7 DFT-calculated structures of H_2S binding in Zr-fum, Zr-mes, and Zr-ita with calculated energies of adsorption ($-\Delta E_{ads}$) indicated. The DFT-calculated structures and energies of H_2O adsorption in all three MOFs are included for comparison. Gray, white, red, yellow, and pale blue spheres correspond to carbon, hydrogen, oxygen, sulfur, and zirconium, respectively.

by comparing the calculated structure for Zr-fum with the previously reported single-crystal X-ray diffraction structure (ESI Fig. S86†).[39] As expected, H_2S was found to preferentially bind within the tetrahedral cavities of all three frameworks (Fig. 7, top; see ESI Fig. S89† for space-filling model). Comparing the activated and H_2S-bound structures yielded 0 K adsorption energies ($-\Delta E_{ads}$) of 41, 44, and 43 kJ mol^{-1} for Zr-fum, Zr-mes, and Zr-ita, respectively, which are comparable to the experimental enthalpies of adsorption (Fig. 4). The H_2S molecules are predicted to be anchored within the tetrahedral cavities by O–H···S interactions with the OH^- groups on the Zr_6 clusters (2.16–2.43 Å in length). Additional hydrogen-bonding interactions between adjacent H_2S molecules are predicted, with S–H···S distances ranging from 2.38 Å to 2.54 Å. Notably, these distances are slightly shorter than the S–H···S distance in $(H_2S)_2$ (2.78 Å),[34] likely due to the increased polarization of H_2S molecules interacting with the framework pores. The favorable packing of H_2S within the tetrahedral cavities accounts for its strong yet reversible adsorption in all three frameworks.

For comparison, we also predicted the preferred binding modes for H_2O in Zr-fum, Zr-mes, and Zr-ita (Fig. 7, bottom). Similar to H_2S, H_2O was found to preferentially bind within the tetrahedral cavities of all three frameworks, albeit with more favorable binding energies in every case. The calculated binding energy for water in Zr-fum ($-\Delta E_{ads}$ = 62 kJ mol^{-1}) is similar to the previously reported experimental enthalpy of adsorption ($-\Delta H_{ads}$ = 60 kJ mol^{-1}),[39] validating our predictions. Notably, the stronger nature of O–H···O interactions compared to S–H···S interactions favors binding additional water molecules within the tetrahedral cavities, leading to a higher predicted uptake in addition to more thermodynamically favorable binding for H_2O over H_2S. The stronger overall binding of H_2O suggests that it should be able to displace H_2S from the tetrahedral cavities of MOFs, providing an avenue to trigger H_2S release under physiological conditions.

H_2S delivery from MOFs

Prior to evaluating the ability of H_2S-loaded Zr-fum, Zr-mes, and Zr-ita to release H_2S under physiologically relevant conditions, we evaluated the stability of these frameworks under aqueous conditions as well as their biocompatibility. Similar to other Zr-MOFs,[57,58] all three frameworks were found to be stable in neutral deionized water (pH 7.0) and cell culture medium (pH 7.4) prepared from Dulbecco's Modified Eagle's Medium (DMEM) supplemented with 10% fetal bovine serum (FBS) over extended periods (3–10 days) (ESI Fig. S73–S75; see ESI Section 13† for details). Based on its high H_2S capacity and stability under physiological conditions, we selected Zr-fum-H_2O as the most promising framework to study further for H_2S delivery. The biocompatibility of Zr-fum-H_2O was assessed by exposing

HeLa cells to varying amounts of activated framework suspended in DMEM supplemented with 10% FBS for 72 h at 37 °C (Fig. 8; see ESI Section 13† for details). Viabilities were determined by incubating the exposed cells with (4,5-dimethylthiazol-2-yl)-2,5-diephenyltetrazolium bromide (MTT) followed by colorimetric quantification in comparison with cells that were not treated with MOF (100% viability).[59] Near 100% viabilities were observed up to concentrations of 0.2 mg mL^{-1}, and >90% viability was observed for Zr-fum-H_2O at concentrations as high as 0.5 mg mL^{-1}. This is in contrast to other MOFs such as Zn-MOF-74, which was found to be highly toxic to HeLa cells at concentrations greater than 0.1 mg mL^{-1} (ESI Fig. S101†).[60] Assuming Zr-fum-H_2O is capable of delivering 4 μmol of H_2S per mg of MOF (Fig. 3), a concentration of 0.1 mg mL^{-1} corresponds to a deliverable concentration of H_2S of up to 400 μM, which is comparable to or above endogenous concentrations (*e.g.*, 50–160 μM in the brain).[7] This highlights the potential benefit in using a porous solid to deliver H_2S: low concentrations (<0.1 mg mL^{-1}) of framework can be employed to release therapeutic levels of H_2S, minimizing any potential side effects from the framework itself. Promisingly, our results suggest that Zr-mes and Zr-ita are also relatively non-toxic to HeLa cells (ESI Fig. S80†).

Having established the biocompatibility of Zr-fum-H_2O, we next evaluated its ability to release H_2S upon subjection to aqueous solution (Fig. 9 and 10). First, a known amount of H_2S-dosed MOF was submerged into a large volume of phosphate buffered saline (PBS) with stirring (~1 mg MOF per mL PBS). Aliquots from the suspension were quenched with a large excess (>20 equiv.) of the fluorescent probe 1,5-dansyl azide (DNS-az), which exhibits rapid turn-on fluorescence ($\lambda_{max} = 520$ nm) upon reaction with H_2S.[61] The release of H_2S from H_2S–Zr-fum-H_2O into PBS was reproducibly confirmed by fluorescence spectroscopy (Fig. 9, upper; ESI Fig. S78†). The concentration of H_2S in solution reached saturation in approximately 30 seconds; given the large excess of free DNS-az present in solution, this suggests

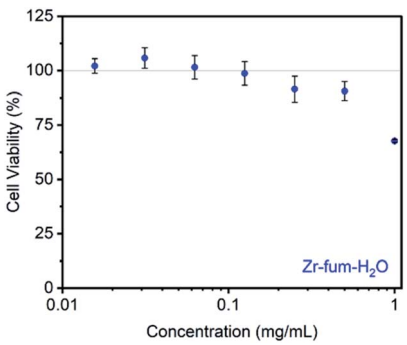

Fig. 8 Viability of HeLa cells upon exposure to suspensions of activated Zr-fum-H_2O at a range of concentrations in DMEM supplemented with 10% FBS for 72 h at 37 °C. Viabilities were determined by incubating the cells with MTT followed by colorimetric analysis using a microplate reader. Results are reported as the average cell viability of 6 wells/concentration compared to untreated cells from three independent trials, with the standard deviation (SD) reported as the error (±SD).

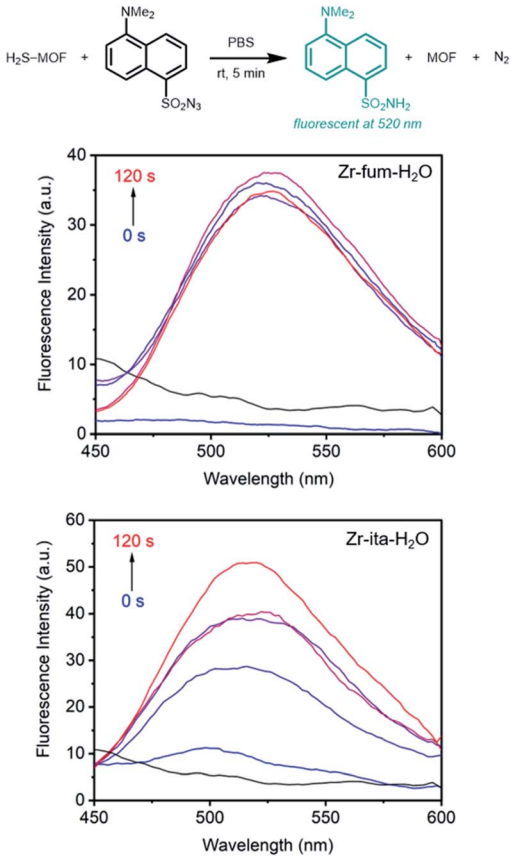

Fig. 9 Fluorescence assay (excitation at 340 nm) using the turn-on fluorescence probe dansyl azide (DNS-az) to confirm the release of H_2S from Zr-fum-H_2O (upper) and Zr-ita-H_2O (lower) upon submersion in phosphate buffered saline (PBS). The black line corresponds to a control experiment lacking MOF. The data were smoothed by adjacent-averaging (15 points).

that the release of H_2S from Zr-fum-H_2O is complete in less than 30 s. Importantly, a control experiment in which H_2S was dosed into a tube lacking MOF and then "poured" into PBS following the same procedure produced no detectable amounts of H_2S, confirming that all of the H_2S was released from Zr-fum-H_2O (black line, Fig. 9). We also reproducibly confirmed the release of H_2S from H_2S–Zr-ita-H_2O using the same assay (Fig. 9, lower; Fig. S79†). In contrast to Zr-fum-H_2O, H_2S release from Zr-ita-H_2O took 120 s to reach saturation, indicating that H_2S release from Zr-ita-H_2O may be slower than from Zr-fum-H_2O. Unfortunately, due to unavoidable loss of gaseous H_2S to air this assay cannot be used to reliably quantify the concentration of H_2S released into solution.

Notably, while the release of H_2S from Zr-fum-H_2O and Zr-ita-H_2O into PBS is relatively rapid, H_2S release under ambient conditions from all three MOFs is quite slow. As assessed by exposure to strips of filter paper soaked in lead chloride solution, all three frameworks were found to still contain H_2S after standing for at least four days in humid air, with Zr-fum-H_2O still containing H_2S after six days in humid air (ESI Fig. S81–S83†). In contrast, both $Na_2S \cdot 9H_2O$ and NaSH were found to completely hydrolyze and degrade in less than 5 h under

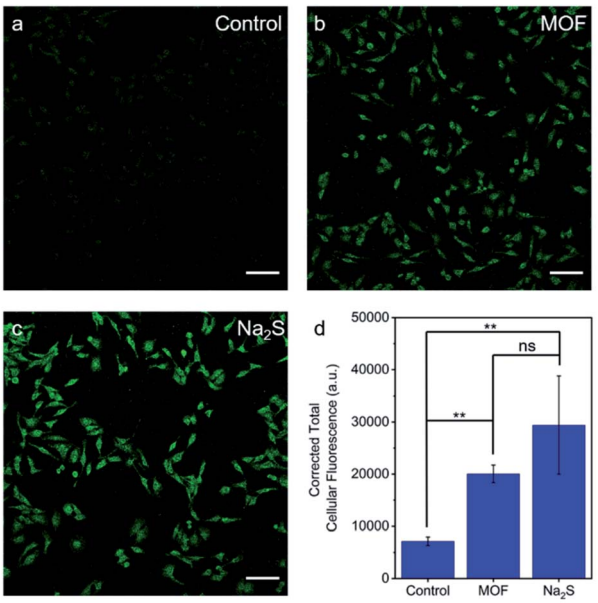

Fig. 10 Representative fluorescence microscopy images of H_2S release in WSP5-loaded HeLa cells treated with (a) water, (b) 0.05 mg mL^{-1} H_2S–Zr-fum-H_2O, or (c) 200 μM Na_2S for 1 h at 37 °C. (d) Quantification of total cellular fluorescence of HeLa cells incubated under the conditions described. The scale bar indicates 100 μm. ns indicates not significant, ** indicates $p < 0.01$.

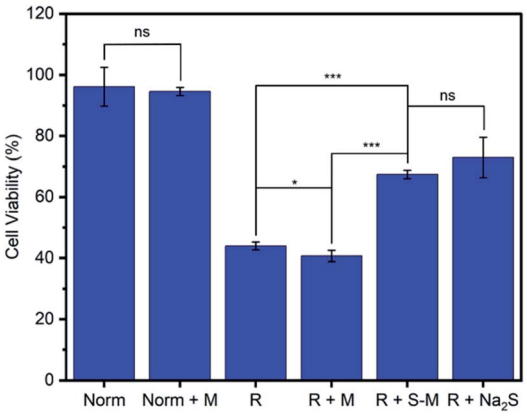

Fig. 11 Hypoxia-reoxygenation model of ischemia-reperfusion injury using H9c2 rat cardiomyoblast cells to confirm the ability of Zr-fum-H_2O to delivery H_2S under physiological conditions. Norm = normoxic conditions; Norm + M = normoxic conditions with activated MOF; R = hypoxia followed by normoxic conditions, simulating reperfusion injury; R + MOF = hypoxia followed by normoxic conditions with activated MOF; R + S–M = hypoxia followed by normoxic conditions with H_2S-loaded Zr-fum-H_2O; R + Na_2S = hypoxia followed by normoxic conditions with $Na_2S \cdot 9H_2O$. * indicates $p < 0.05$, *** indicates $p < 0.001$, and ns indicates not significant.

ambient conditions (Fig. S84†). The clean release of H_2S into water and the long-term stability of these MOFs in humid air makes them ideal solid sources of H_2S that can be easily handled in the laboratory.[9]

The ability of H_2S–Zr-fum-H_2O to deliver H_2S to cells under physiologically-relevant conditions was further probed using confocal fluorescence microscopy (Fig. 10). Specifically, HeLa cells were incubated first with DMEM containing WSP5 (WSP = Washington State Probe), a selective fluorescence probe for intracellular H_2S,[62] followed by rinsing and exposure to water (Fig. 10a), H_2S–Zr-fum-H_2O (Fig. 10b), or $Na_2S \cdot 9H_2O$ (Fig. 10c). For both H_2S–Zr-fum-H_2O and $Na_2S \cdot 9H_2O$, a statistically significant enhancement in corrected total cellular fluorescence (CTCF) was observed compared to the control experiment, validating the release and cellular uptake of H_2S in both cases. Together, these fluorescence experiments (Fig. 9 and 10) confirm the ability of H_2S–Zr-fum-H_2O to release H_2S under physiologically relevant conditions for subsequent uptake by cells.

One of the primary proposed therapeutic modes of H_2S is its ability to mediate oxidative stress within cells.[13,63] For example, H_2S has been shown to limit the oxidative damage to tissue that occurs following the temporary blockage of blood flow during a stroke or myocardial infarction when a period of ischemia or hypoxia is followed by a return of normoxic blood flow, known as ischemia-reperfusion injury (R).[63,64] We evaluated the ability of Zr-fum-H_2O to deliver H_2S and mitigate reperfusion injury using an *in vitro* model of this condition, hypoxia-reoxygenation, in H9c2 rat cardiomyoblast cells (Fig. 11). As expected, cardiomyoblast cells incubated under normoxic conditions in the absence (Norm) or presence of desolvated Zr-fum-H_2O (Norm + M) demonstrated similar viabilities (96 ± 6% and 94 ± 1%, respectively). The latter result is consistent with the lack of toxicity observed for this material with HeLa cells (Fig. 9). In contrast, cells incubated under hypoxic conditions (5% CO_2 in N_2 for 10 minutes) followed by a return to normoxic conditions, simulating a reperfusion injury (R), demonstrated significantly reduced viabilities (44 ± 1%). However, subjecting cells to this reperfusion injury model in the presence of H_2S–Zr-fum-H_2O (R + S–M) led to a significant improvement in their viabilities (67 ± 1%), confirming the potential of Zr-fum-H_2O as a delivery vessel for therapeutic H_2S. Importantly, the presence of activated MOF (R + M) did not lead to an increase in viability compared to cells in the absence of MOF (41 ± 1%), corroborating that the therapeutic value of H_2S–Zr-fum-H_2O is likely due to H_2S release. Likewise, a statistically identical improvement in cell viabilities (73 ± 7%) was observed using $Na_2S \cdot 9H_2O$ in place of H_2S–Zr-fum-H_2O (R + Na_2S), confirming that H_2S-loaded MOFs provide similar therapeutic value as traditional sources of H_2S but with enhanced stability in the solid state. Overall, our results suggest that Zr-fum-H_2O, as well as Zr-mes-H_2O and Zr-ita-H_2O, represent promising vehicles for the delivery of biologically active H_2S under physiological conditions.

Conclusions

The controlled delivery of H_2S is an unsolved challenge in medicine and biology.[9] Here, we demonstrate that biocompatible MOFs that are completely stable to H_2S, including Zr-fum, Zr-mes, and Zr-ita, present a promising new direction for the design of vehicles for H_2S release under physiological

conditions. In particular, given its excellent stability, high H_2S capacity, lack of toxicity, ambient stability, and performance in a cellular hypoxia-reoxygenation injury assay, Zr-fum-H_2O represents a next-generation platform for the therapeutic delivery of H_2S. In addition to Zr-fum-H_2O, this work also adds Zr-mes-H_2O and Zr-ita-H_2O to the growing lexicon of biocompatible MOFs for drug delivery applications. Future work will focus on functionalizing the surface of these frameworks to further control the rate and location of H_2S delivery under physiological conditions.

Author contributions

P. J. M., J. J. Wilson, R. M. M., F. E. C., and J. J. Woods conceived the project. R. M. M. and F. E. C. synthesized and characterized MOFs and carried out all gas adsorption measurements. J. J. Woods carried out all cellular experiments with assistance from R. M. M. J.-H. L. carried out DFT calculations. J. K. designed the DRIFTS cell and carried out experiments with assistance from R. M. M. J. H. H. preliminarily optimized the synthesis of MOFs. J. J. F.-R. carried out SEM measurements. The final version of the manuscript was written with contributions from all co-authors.

Conflicts of interest

P. J. M. is listed as a co-inventor on several patents that include functionalized metal–organic frameworks.

Acknowledgements

We thank Cornell University for initial financial support of this work. Further support for this work was provided by the National Institute of General Medical Sciences of the National Institutes of Health under award number R35GM138165 (F. E. C., R. M. M., J. K., J. J. F. R., P. J. M.). The content is solely the responsibility of the authors and does not necessarily represent the official views of the National Institutes of Health. We are grateful to Cornell University for providing a Summer Experience Grant to F. E. C. We thank the American Heart Association for providing a predoctoral fellowship to J. J. Woods (20PRE35120390). Computational work and resources were supported by the KIST Institutional Program (Project No. 2E30460) and KISTI Supercomputing Centre (Project No. KSC-2020-CRE-0189) (J.-H. L). This work made use of the Cornell Center for Materials Research Shared Facilities, which are supported through the NSF MRSEC program (DMR-1719875). ^{1}H NMR data were collected on a Bruker INOVA 500 MHz spectrometer that was purchased with support from the NSF (CHE-1531632). Imaging data was acquired through the Cornell University Biotechnology Resource Center, which is supported in part by the NIH (S10RR025502). The purchase of the diffuse reflectance IR cell used was supported by the Kavli Institute at Cornell for Nanoscale Science.

Notes and references

1 M. Khabazipour and M. Anbia, *Ind. Eng. Chem. Res.*, 2019, **58**, 22133–22164.
2 M. S. Shah, M. Tsapatsis and J. I. Siepmann, *Chem. Rev.*, 2017, **117**, 9755–9803.
3 X. Zhang, Y. Tang, S. Qu, J. Da and Z. Hao, *ACS Catal.*, 2015, **5**, 1053–1067.
4 V. Garcia-Arriaga, J. Alvarez-Ramirez, M. Amaya and E. Sosa, *Corros. Sci.*, 2010, **52**, 2268–2279.
5 K. Qu, S. W. Lee, J. S. Bian, C.-M. Low and P. T.-H. Wong, *Neurochem. Int.*, 2008, **52**, 155–165.
6 G. Yang, L. Wu, B. Jiang, W. Yang, J. Qi, K. Cao, Q. Meng, A. K. Mustafa, W. Mu, S. Zhang, S. H. Snyder and R. Wang, *Science*, 2008, **322**, 587–590.
7 K. Abe and H. Kimura, *J. Neurosci.*, 1996, **16**, 1066–1071.
8 X. Cao, L. Ding, Z. Xie, Y. Yang, M. Whiteman, P. K. Moore and J.-S. Bian, *Antioxid. Redox Signaling*, 2019, **31**, 1–38.
9 C. R. Powell, K. M. Dillon and J. B. Matson, *Biochem. Pharmacol.*, 2018, **149**, 110–123.
10 S. Sestito, G. Nesi, R. Pi, M. Macchia and S. Rapposelli, *Front. Chem.*, 2017, **5**, 72.
11 X. Cao, L. Cao, L. Ding and J. Bian, *Mol. Neurobiol.*, 2017, **55**, 3789–3799.
12 J. L. Wallace and R. Wang, *Nat. Rev. Drug Discovery*, 2015, **14**, 329–345.
13 Z. J. Song, M. Y. Ng, Z.-W. Lee, W. Dai, T. Hagen, P. K. Moore, D. Huang, L.-W. Deng and C.-H. Tan, *MedChemComm*, 2014, **5**, 557–570.
14 D. J. Lefer, *Proc. Natl. Acad. Sci. U. S. A.*, 2007, **104**, 17907–17908.
15 C. Szabó, *Nat. Rev. Drug Discovery*, 2007, **6**, 917–935.
16 J. J. Woods and J. J. Wilson, *Angew. Chem., Int. Ed.*, 2021, **60**, 1588–1592.
17 J. J. Woods, J. Cao, A. R. Lippert and J. J. Wilson, *J. Am. Chem. Soc.*, 2018, **140**, 12383–12387.
18 Y. Sun, L. Zheng, Y. Yang, X. Qian, T. Fu, X. Li, Z. Yang, H. Yan, C. Cui and W. Tan, *Nano-Micro Lett.*, 2020, **12**, 103.
19 L. Wang, M. Zheng and Z. Xie, *J. Mater. Chem. B*, 2018, **6**, 707–717.
20 R. C. Huxford, J. Della Rocca and W. Lin, *Curr. Opin. Chem. Biol.*, 2010, **14**, 262–268.
21 N. J. Hinks, A. C. McKinlay, B. Xiao, P. S. Wheatley and R. E. Morris, *Microporous Mesoporous Mater.*, 2010, **129**, 330–334.
22 P. K. Allan, P. S. Wheatley, D. Aldous, M. I. Mohideen, C. Tang, J. A. Hriljac, I. L. Megson, K. W. Chapman, G. De Weireld, S. Vaesen and R. E. Morris, *Dalton Trans.*, 2012, **41**, 4060.
23 K. Vikrant, V. Kumar, Y. S. Ok, K.-H. Kim and A. Deep, *TrAC, Trends Anal. Chem.*, 2018, **105**, 263–281.
24 J. Liu, Y. Wei, P. Li, Y. Zhao and R. Zou, *J. Phys. Chem. C*, 2017, **121**, 13249–13255.
25 H. Jo, W. R. Lee, N. W. Kim, H. Jung, K. S. Lim, J. E. Kim, D. W. Kang, H. Lee, V. Hiremath, J. G. Seo, H. Jin,

D. Moon, S. S. Han and C. S. Hong, *ChemSusChem*, 2017, **10**, 541–550.
26 O. Shekhah, Y. Belmabkhout, K. Adil, P. M. Bhatt, A. J. Cairns and M. Eddaoudi, *Chem. Commun.*, 2015, **51**, 13595–13598.
27 B. Supronowicz, A. Mavrandonakis and T. Heine, *J. Phys. Chem. C*, 2013, **117**, 14570–14578.
28 C. Petit and T. J. Bandosz, *Dalton Trans.*, 2012, **41**, 4027.
29 C. Petit, B. Mendoza and T. J. Bandosz, *ChemPhysChem*, 2010, **11**, 3678–3684.
30 L. Hamon, C. Serre, T. Devic, T. Loiseau, F. Millange, G. Férey and G. D. Weireld, *J. Am. Chem. Soc.*, 2009, **131**, 8775–8777.
31 S. Vaesen, V. Guillerm, Q. Yang, A. D. Wiersum, B. Marszalek, B. Gil, A. Vimont, M. Daturi, T. Devic, P. L. Llewellyn, C. Serre, G. Maurin and G. De Weireld, *Chem. Commun.*, 2013, **49**, 10082.
32 A. J. Rieth, A. M. Wright and M. Dincă, *Nat. Rev. Mater.*, 2019, **4**, 708–725.
33 E. Sánchez-González, P. G. M. Mileo, M. Sagastuy-Breña, J. R. Álvarez, J. E. Reynolds, A. Villarreal, A. Gutiérrez-Alejandre, J. Ramírez, J. Balmaseda, E. González-Zamora, G. Maurin, S. M. Humphrey and I. A. Ibarra, *J. Mater. Chem. A*, 2018, **6**, 16900–16909.
34 A. Das, P. K. Mandal, F. J. Lovas, C. Medcraft, N. R. Walker and E. Arunan, *Angew. Chem., Int. Ed.*, 2018, **57**, 15199–15203.
35 A. J. Rieth, A. M. Wright, G. Skorupskii, J. L. Mancuso, C. H. Hendon and M. Dincă, *J. Am. Chem. Soc.*, 2019, **141**, 13858–13866.
36 H. Kim, S. Yang, S. R. Rao, S. Narayanan, E. A. Kapustin, H. Furukawa, A. S. Umans, O. M. Yaghi and E. N. Wang, *Science*, 2017, **356**, 430–434.
37 J. Canivet, A. Fateeva, Y. Guo, B. Coasne and D. Farrusseng, *Chem. Soc. Rev.*, 2014, **43**, 5594–5617.
38 N. C. Burtch, H. Jasuja and K. S. Walton, *Chem. Rev.*, 2014, **114**, 10575–10612.
39 H. Furukawa, F. Gándara, Y.-B. Zhang, J. Jiang, W. L. Queen, M. R. Hudson and O. M. Yaghi, *J. Am. Chem. Soc.*, 2014, **136**, 4369–4381.
40 I. C. Smith and B. L. Carson, *Trace metals in the environment*, Ann Arbor Science Publishers, Ann Arbor, MI, 1978, vol. 3 – Zirconium.
41 G. Aquilina, A. Bach, V. Bampidis, M. D. Lourdes Bastos, G. Flachowsky, J. Gasa-Gasó, M. Gralak, C. Hogstrand, L. Leng, S. López-Puente, G. Martelli, B. Mayo, D. Renshaw, G. Rychen, M. Saarela, K. Sejrsen, P. V. Beelen, R. J. Wallace and J. Westendorf, *EFSA J.*, 2013, **11**, 14.
42 C. W. Song, D. I. Kim, S. Choi, J. W. Jang and S. Y. Lee, *Biotechnol. Bioeng.*, 2013, **110**, 2025–2034.
43 I. Abánades Lázaro, S. Haddad, J. M. Rodrigo-Muñoz, R. J. Marshall, B. Sastre, V. del Pozo, D. Fairen-Jimenez and R. S. Forgan, *ACS Appl. Mater. Interfaces*, 2018, **10**, 31146–31157.
44 M. Sk, S. Bhowal and S. Biswas, *Eur. J. Inorg. Chem.*, 2015, **2015**, 3317–3322.
45 J. Wang and K. Zhang, *Metab. Eng.*, 2015, **30**, 190–196.
46 T. Cordes, A. Michelucci and K. Hiller, *Annu. Rev. Nutr.*, 2015, **35**, 451–473.
47 T. Klement and J. Büchs, *Bioresour. Technol.*, 2013, **135**, 422–431.
48 H. Reinsch, S. Waitschat, S. M. Chavan, K. P. Lillerud and N. Stock, *Eur. J. Inorg. Chem.*, 2016, **2016**, 4490–4498.
49 S. K. Murthy, *Int. J. Nanomed.*, 2007, **2**, 129–141.
50 T. D. Bennett and A. K. Cheetham, *Acc. Chem. Res.*, 2014, **47**, 1555–1562.
51 C. E. Bien, K. K. Chen, S.-C. Chien, B. R. Reiner, L.-C. Lin, C. R. Wade and W. S. W. Ho, *J. Am. Chem. Soc.*, 2018, **140**, 12662–12666.
52 J. A. Zárate, E. Sánchez-González, T. Jurado-Vázquez, A. Gutiérrez-Alejandre, E. González-Zamora, I. Castillo, G. Maurin and I. A. Ibarra, *Chem. Commun.*, 2019, **55**, 3049–3052.
53 L. Hamon, H. Leclerc, A. Ghoufi, L. Oliviero, A. Travert, J.-C. Lavalley, T. Devic, C. Serre, G. Férey, G. De Weireld, A. Vimont and G. Maurin, *J. Phys. Chem. C*, 2011, **115**, 2047–2056.
54 P. E. Blöchl, *Phys. Rev. B: Condens. Matter Mater. Phys.*, 1994, **50**, 17953–17979.
55 G. Kresse and D. Joubert, *Phys. Rev. B: Condens. Matter Mater. Phys.*, 1999, **59**, 1758–1775.
56 S. Grimme, S. Ehrlich and L. Goerigk, *J. Comput. Chem.*, 2011, **32**, 1456–1465.
57 D. Bůžek, J. Demel and K. Lang, *Inorg. Chem.*, 2018, **57**, 14290–14297.
58 C. G. Piscopo, A. Polyzoidis, M. Schwarzer and S. Loebbecke, *Microporous Mesoporous Mater.*, 2015, **208**, 30–35.
59 T. Mosmann, *J. Immunol. Methods*, 1983, **65**, 55–63.
60 À. Ruyra, A. Yazdi, J. Espín, A. Carné-Sánchez, N. Roher, J. Lorenzo, I. Imaz and D. Maspoch, *Chem.–Eur. J.*, 2015, **21**, 2508–2518.
61 H. Peng, Y. Cheng, C. Dai, A. L. King, B. L. Predmore, D. J. Lefer and B. Wang, *Angew. Chem., Int. Ed.*, 2011, **50**, 9672–9675.
62 B. Peng, W. Chen, C. Liu, E. W. Rosser, A. Pacheco, Y. Zhao, H. C. Aguilar and M. Xian, *Chem.–Eur. J.*, 2014, **20**, 1010–1016.
63 J. W. Calvert, W. A. Coetzee and D. J. Lefer, *Antioxid. Redox Signaling*, 2010, **12**, 1203–1217.
64 D. Wu, J. Wang, H. Li, M. Xue, A. Ji and Y. Li, *Oxid. Med. Cell. Longevity*, 2015, **2015**, 1–16.